THE JOURNAL OF PHYSICAL CHEMISTRY C

Article

Cite This: J. Phys. Chem. C 2018, 122, 29598−29606

pubs.acs.org/JPCC

Monitoring the Photothermal Reshaping of Individual Plasmonic Nanorods with Coherent Mechanical Oscillations

Fabricio Della Picca,[†] Marina V. Gutiérrez,[‡] Andrea V. Bragas,[†,§] and Alberto F. Scarpettini*[,‡,∥]

[†]Departamento de Física, Facultad de Ciencias Exactas y Naturales, Universidad de Buenos Aires, 1428 Buenos Aires, Argentina

[‡]Facultad Regional Delta, Universidad Tecnológica Nacional, 2804 Campana, Provincia de Buenos Aires, Argentina

[§]IFIBA, UBA-CONICET, 1428 Buenos Aires, Argentina

[∥]Consejo Nacional de Investigaciones Científicas y Técnicas (CONICET), 1425 Buenos Aires, Argentina

ABSTRACT: Light absorption in gold nanoparticles leads to metal heating that induces photothermal reshaping because of atomic surface diffusion at temperatures well below the gold melting point. In this work, we perform time-resolved experiments to measure the frequencies of the extensional coherent mechanical mode in single gold nanorods, as a monitor of the changes in their aspect ratio produced by this photoinduced reshaping. We show that photothermal reshaping always occurs in typical pump−probe experiments conducted in air even at low-excitation light irradiance and usually long measuring times. The reshaping effect can be reduced by a polymer coating, which allows faster heat dissipation from the nanoparticle to the environment.

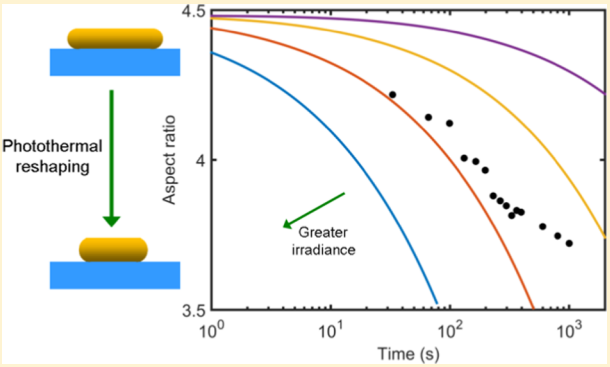

INTRODUCTION

In recent years, a well-established theoretical description was formulated about the thermodynamics of metal nanoparticles immersed in a dissipative medium and illuminated by a continuous wave (CW) or an ultrashort-pulsed laser.[1−4] In a continuous absorption regime, the steady-state temperature profile is reached after a transient evolution with two characteristic time scales, associated with heat diffusion in gold and in the environment, respectively. The thermalization inside the nanoparticle occurs much faster than in the surrounding medium. Thus, the establishment of the temperature profile of the overall system is governed by the medium diffusivity. On the other hand, in the femtosecond-pulsed illumination case, the incident energy is absorbed by the free-electron gas, which thermalizes very fast over the pulse time scale. Subsequently, this hot electronic gas cools down through electron−phonon interactions on the order of picoseconds (for not too small nanoparticles), whereas the nanoparticle is in internal equilibrium at a uniform temperature, but not with the surrounding medium that is still at the initial room temperature. The final energy diffusion to the environment occurs at a higher characteristic time scale (nanoseconds), usually smaller than or comparable with the pulse repetition rate, which leads to a cooling of the nanoparticle and a heating of the surrounding medium. Baffou et al. presented analytical and numerical approaches of heat release of gold nanospheres immersed in water and illuminated by a femtosecond-pulsed laser at their plasmonic resonance.[1]

Additionally, ultrafast laser excitation of metal nanoparticles drives the coherent excitation of their vibrational modes lying in the frequency range of gigahertz to terahertz.[4−7] The measured vibrational frequencies provide a way of determining the material properties of nanometer-sized objects as well as the viscoelastic properties of the surrounding medium.[8−10] Vibrational modes depend on the shape, size, crystal structure, and local environment of the nanoparticle.[3,4,11,12] As any fluctuation in the size and/or the aspect ratio (AR) of the gold nanorod (GNR) will necessarily have an impact on the mechanical frequency value, it is possible to use this measurement in sensitive monitoring of the changes that the heating could cause on individual GNRs. Indeed, many authors show morphological changes in GNR due to the diffusion of the surface atoms produced by photothermal heating, through the observation of shifts in their localized surface plasmon resonance (LSPR) peaks and decrements of the GNR aspect ratios observed in electron microscopy images.[13−21]

In this work, we study the photothermal reshaping process of single GNRs through the tracing of the extensional mechanical mode frequency under ultrashort-pulsed light excitation. We show a numerical description of the value of the initial instantaneous temperature increment, the time scales governing the heat release into the surroundings, the spatial extension of the temperature distribution in the surrounding medium, the geometric profile reshaping process, and the aspect ratio decrease during the laser repetition period and at longer irradiation times. Finally, we show that this photo-

Received: September 27, 2018
Revised: November 30, 2018
Published: December 3, 2018

DOI: 10.1021/acs.jpcc.8b09458
J. Phys. Chem. C 2018, 122, 29598−29606

thermal reshaping can be drastically reduced by embedding the nanoparticle in a viscoelastic medium.

METHODS

Sample Preparation and Optical and Morphological Characterization. *Materials.* All chemicals were obtained from commercial suppliers and used without further purification. Gold(III) chloride trihydrate ($HAuCl_4 \cdot 3H_2O$, ≥99.9%), hexadecyltrimethylammonium bromide (CTAB, ≥99%), sodium borohydride ($NaBH_4$, ≥98%), sodium oleate (NaOl, ≥99%), silver nitrate ($AgNO_3$, ≥99%), (3-amino-propyl)-trimethoxysilane (APTMS, ≥97%), and poly(sodium 4-styrenesulfonate) (PSS, average $M_w \approx 70\,000$) were purchased from Sigma-Aldrich. Ascorbic acid (≥99.7%) and hydrochloric acid (HCl, 37 wt % in water) were purchased from Biopack. Poly(methyl methacrylate) (PMMA) was purchased from MicroChem. Glass microscope slides were purchased from Marienfeld. Ultrapure water obtained from a Millipore Direct-Q 3 UV system was used in the experiments.

Synthesis of GNRs. Gold nanorods were synthesized by seed-mediated growth.[22] To prepare the seed solution, 5 mL of 0.5 mM $HAuCl_4$ was mixed with 5 mL of 0.2 M CTAB solution, and then 1 mL of fresh 6 mM $NaBH_4$ was injected into the Au(III)−CTAB solution under vigorous stirring. This seed solution was stirred 2 min and then aged at room temperature for 30 min before use. To prepare the growth solution, 900 mg of CTAB and 123.4 mg of NaOl were dissolved in 25 mL of warm water (50 °C). The solution was allowed to cool down to 30 °C, and 2.4 mL of 4 mM $AgNO_3$ solution was added. After 15 min, 25 mL of 1 mM $HAuCl_4$ solution was added. The solution became colorless after 90 min of stirring, and 0.36 mL of HCl (37 wt % in water) was then introduced to adjust the pH. After another 15 min of slow stirring, 0.125 mL of 0.064 M ascorbic acid was added, and the solution was vigorously stirred for 30 s. Finally, 0.001 mL of seed solution was injected into the growth solution. The resultant mixture was stirred for 30 s and left undisturbed at 30 °C for 12 h for GNR growth. This protocol gives monodisperse and stable gold nanorods, stabilized by a bilayer of CTAB and NaOl. To remove excess CTAB, the final solution was purified by three centrifugations at 7000 rpm for 30 min, followed by careful removal of the supernatant. The precipitates were redispersed in deionized water.

Immobilization of GNRs. Glass microscope slides were first cleaned with deionized water in an ultrasonic bath for 30 min. They were then immersed in 5% hydrofluoric acid for 30 s and washed with deionized water. Then, slides were immersed in APTMS aqueous solution (1:100, pH 10) in a dark environment for 1 h at room temperature. They were then thoroughly rinsed with deionized water and isopropyl alcohol to remove any physisorbed APTMS. After this procedure, the glasses were immersed in a solution of 20 mg/mL PSS for 1 h and rinsed again with deionized water and isopropyl alcohol. They were finally immersed into the purified GNR solution for 4 h; kept at room temperature, without applying any mixing; and then washed and dried. For the covering with PMMA, the sample was spin-coated at 3000 rpm for 2 min and then baked at 160 °C for 3 min.

Structural and Optical Characterization. The extinction spectra were measured with a UV/vis spectrophotometer (Mecasys, Optizen Pop). Images of GNRs on the graphite substrate were taken by a field emission scanning electron microscope (SEM, Zeiss Supra 40) operating at 3 kV. GNR lengths and diameters were measured from SEM images to obtain size and aspect ratio (AR) statistics.

Single-Particle Pump−Probe Measurements. The second harmonic (at 400 nm) of a Ti:Sapphire laser with a repetition rate, f_r, of 95 MHz, with a pulse width of 100 fs, and modulated with an acousto-optic modulator is used as the pump. A weak probe is set at 800 nm and sent to the sample after passing through the optical delay line. Both beams are focused using a high-numerical-aperture microscope objective onto a single GNR with a pump (probe) spot size diameter of 0.4 μm (0.8 μm). The signal is collected in transmission mode after optical filtering and sent to a lockin amplifier.

RESULTS AND DISCUSSION

Aqueous solutions of monodisperse GNRs were obtained by a seed-mediated growth, as described in the Methods section, and then purified three times. Then, the GNRs were immobilized on chemically modified glass slides,[23] in a way that the particles were far enough away from each other, for their use in single-particle pump−probe experiments. Figure 1

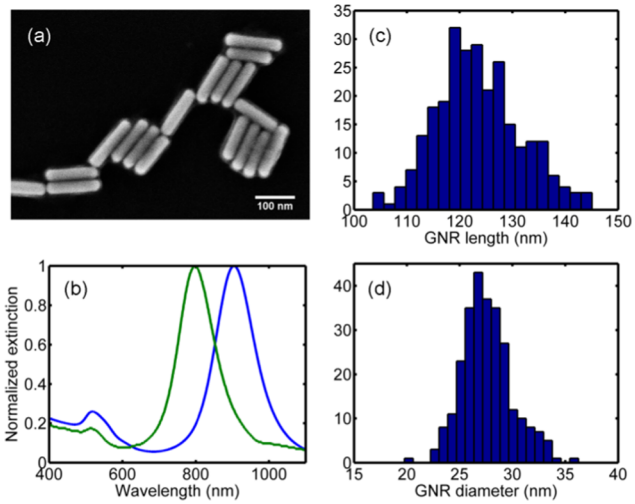

Figure 1. (a) SEM image of the synthesized GNRs disposed on the graphite surface. (b) Extinction spectra of the colloid aqueous solution (blue) and GNRs on glass slides surrounded by air (green). The blue shift of the longitudinal LSPR is due to a lower effective refraction index with respect to water. (c, d) Histograms of the length, L, and diameter, d, of GNRs measured from SEM images. Average values with standard deviation are 123.5 ± 8.0 and 27.7 ± 2.3 nm, respectively.

shows a representative SEM image of the GNRs (with density greater than the one used in the pump−probe experiments) and extinction spectra of the colloid aqueous solution and of the GNRs on glass as well. The decrease of the medium effective permittivity of GNRs on glass slides and surrounded by air, with respect to that of water, causes a blue shift of the longitudinal resonance peak from around 900 nm toward 800 nm, which is located near the Ti:Sapphire laser wavelength. Measurements on hundreds of GNRs from SEM images give an average length of 123.5 ± 8.0 nm and an average diameter of 27.7 ± 2.3 nm. Normal distributions of these nanorod dimension measurements are shown in Figure 1c,d. These values give an average aspect ratio of 4.49 ± 0.42.

Mechanical Oscillations. It is well known that the position of the LSPR (optical) in GNRs depends on their

DOI: 10.1021/acs.jpcc.8b09458
J. Phys. Chem. C 2018, 122, 29598−29606

aspect ratio.[24,25] From the point of view of the mechanical oscillations, the length, L, is the most relevant parameter when defining the extensional mode, whereas the diameter, d, is the one that defines the breathing mode frequency.[3,11] In GNRs, the extensional mode, in which there is a periodic contraction and extension of the major axis of the GNR, produces the highest signal in pump−probe experiments if the wavelength of the probe is located near the maximum of the longitudinal LSPR. In this work, our measurements and analysis only focus on the extensional mode. The description of this oscillation in a continuous medium can be simplified by a one-dimensional partial differential equation in the coordinate $u(x, t)$ with no external forces

$$\rho A\frac{\partial^2 u}{\partial t^2} = \frac{\partial}{\partial x}\left(EA\frac{\partial u}{\partial x}\right) \quad (1)$$

where ρ is mass density (19.3 g/cm^3 for gold), A is the geometric cross section, and E is the Young modulus (42 GPa in the [100] growth direction). If we assume that A and E are constants along the axis, eq 1 reduces to $\partial^2u/\partial t^2 = c^2\partial^2u/\partial x^2$, where $c = \sqrt{E/\rho}$. The oscillation modes that correspond to a rod of length L whose both ends are stress-free have natural frequencies as

$$\omega_j = j\frac{\pi}{L}\sqrt{\frac{E}{\rho}} \quad (2)$$

Usually, only the first mode (j = 1) is detectable in pump−probe experiments. The Young modulus E used in this model considers only the restitutive force exerted by a pure elastic gold nanorod. A more accurate model needs to consider gold internal friction, external viscoelastic environment, and clamping to the substrate.[12,26] Considering that the internal friction would allow us to define a finite quality factor, Q, for the oscillator but that it does not affect the value of the frequency at all, it is not a relevant parameter for the analysis in this work. In the same way, the viscoelastic character of the environment will only be considered toward the end while comparing the results obtained for the GNRs when they are immersed in a polymer such as PMMA. However, the anchoring to the substrate does play a role in determining the frequency of the extensional oscillation because it adds an extra restoring force to the system. Indeed, this additional restoring force can be inferred from the measured frequencies and included in the effective Young modulus E_{eff}. Using eq 2 and correlating the histogram of GNR lengths in Figure 1c with the histogram of the extensional frequencies measured at the beginning (GNRs in air over a glass substrate), an equivalent elastic modulus of 12 GPa must be added to E. Then, E_{eff} = 54 GPa was used for all of the calculations in this work.

Single GNRs were excited with a pump pulse from a doubled Ti:Sapphire oscillator tuned near the interband transition energy in gold (400 nm wavelength) and probed with a lower-power pulse at the longitudinal LSPR (about 800 nm). The transmitted light was recorded as a function of the optical delay of the probe so as to detect the variations produced by the mechanical oscillations in the plasmon band and therefore in the optical transmission, with a resolution of few tens of femtoseconds, allowing the building of the real-time trace of the coherent phonon oscillations. Frequency values reported in this work are extracted from these temporal traces after a specific measurement time that can range from a few tens to hundreds of seconds.

Time evolution of the extensional frequencies of single GNRs was measured during hundreds or thousands of seconds, with irradiance between 0.1 and 2.3 mW/μm^2 in the center of the focal waist. Typical temporal evolution of the frequency of a single GNR is observed in Figure 2a, where the frequency

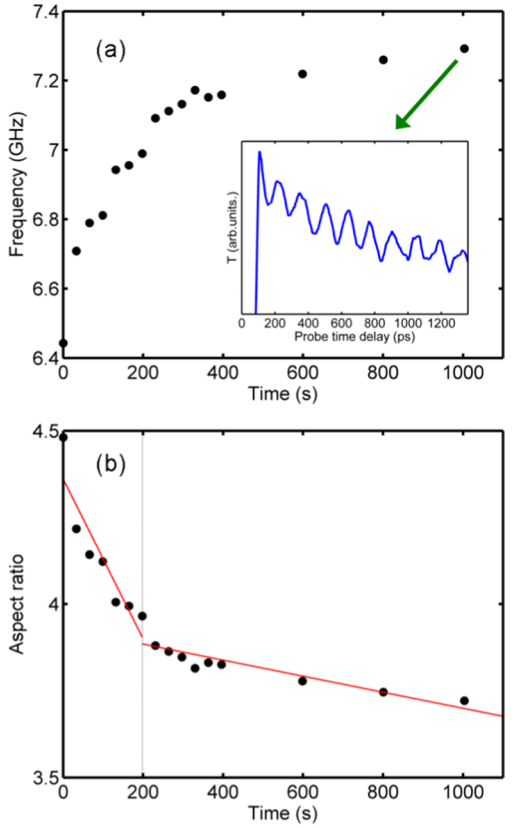

Figure 2. (a) Time evolution of the extensional mechanical frequency of a single GNR on glass surrounded by air and excited with a femtosecond-pulsed laser at 400 nm. Frequency error is 2%. All measured GNRs showed similar behavior. The inset shows a typical time-trace optical transmission signal, corresponding to the last frequency point. (b) Aspect ratio (AR) evolution, calculated from extensional frequency measurements and eq 2, of the same GNR in (a), with an irradiance of 2.3 mW/μm^2 before the vertical dotted line and 1.15 mW/μm^2 after it. The variation in the AR change rate can be seen (red lines are guides to the eye).

grows up monotonically, suggesting a shortening of the GNR. Representative time trace of the optical oscillations corresponding to one of the data points is presented in the inset. Additionally, the pump power decreased after 200 s, from 2.3 to 1.15 mW/μm^2, leading to an evident slope change in the temporal evolution of the GNR aspect ratio, calculated by eq 2 and shown in Figure 2b. As a higher irradiance implies a higher temperature, the graphs shown in Figure 2 suggest that those changes are produced by photothermal reshaping, as will be confirmed in the following sections.

Energy Absorption and Temperature of the Nanorods. It has been a long time since Mullins and co-workers predicted spheroidization of metal nanoparticles due to curvature-induced atomic surface diffusion at ambient temperatures or at very low power laser-induced heating, rather than due to a threshold melting process.[27,28] These morphological

DOI: 10.1021/acs.jpcc.8b09458
J. Phys. Chem. C 2018, 122, 29598−29606

Table 1. Physical Constants Used in this Work for Gold and Different Surrounding Media[a]

parameter	unit	gold	water	air	glass	PMMA
mass density, ρ	(kg/m^3)	19 300	1000	1.2	2520	1180
specific heat capacity, c	(J/(kg K))	129	4181	1012	840	1466
thermal conductivity, κ	(W/(m K))	315	0.6	0.024	0.8	0.2
thermal diffusivity, $\alpha = \kappa/\rho c$	(mm^2/s)	127	0.143	19	0.34	0.116

[a]Specific heat capacity is at constant pressure.

changes are described with a system of partial differential equations on surfaces of revolution under the assumption of isotropy of surface tension and surface self-diffusion coefficient.[27−29] After those predictions, several experiments showed this photothermal phenomenon in different nanosized samples.[13,30,31] Some authors have also reported changes in the extensional frequency of GNRs under pulsed irradiation above a given power threshold.[3,4,9] Taylor et al. showed a photothermal reshaping behavior of GNRs irradiated with femtosecond laser pulses and proposed that the stability abruptly decreases with increasing their aspect ratio.[32] Surface atoms diffuse much easier in larger- than in shorter-aspect-ratio rods, inducing reshaping at any given temperature. This fact has been exploited to promote controlled nanorod reshaping by irradiation with a femtosecond laser, yielding colloids with narrower LSPR bands.[20] It is then worth noticing here that current plasmonic applications that use sharp geometrical features to take advantage of huge field enhancement factors must necessarily consider surface-diffusion-driven shape changes even at low temperatures.

Before studying the surface diffusion in GNRs, we must understand the process of light absorption and conversion into thermal energy, as well as the temperatures reached by the nanoparticle and the environment as a function power and time. We consider a system consisting of a gold nanorod of length L and diameter d centered in a three-dimensional cubic domain representing the surrounding medium. The rod is considered as a cylinder of length L-d and diameter d with two hemispheres of radius $d/2$ at its ends. The nanorod is uniformly illuminated at a frequency $\omega = 2\pi c_0/\lambda n$, where c_0 is the speed of light in vacuum, λ is the light wavelength, and n is the optical refractive index of the medium. If a system that is initially at temperature T_0 absorbs light, the temperature increase T above T_0 at the position r and time t is given by the heat diffusion equation

$$\rho c \partial_t T(r, t) = \kappa \nabla^2 T(r, t) + p(r, t) \tag{3}$$

where c is the specific heat capacity at constant pressure, κ is the thermal conductivity, and $p(r, t)$ is the heat power density, nonzero only inside the nanorod (where the light is absorbed). No fluid convection is considered. For the proposed system, this yields a set of two differential equations (one for the gold nanorod and one for the surrounding medium) with two boundary conditions at the gold−medium interface

$$\begin{cases} \rho_{Au} c_{Au} \partial_t T(r, t) = \kappa_{Au} \nabla^2 T(r, t) + p(r, t) \text{ for } r \in \text{GNR} \\ \rho_m c_m \partial_t T(r, t) = \kappa_m \nabla^2 T(r, t) \text{ for } r \notin \text{GNR} \\ \kappa_m \partial_\perp T(s^+, t) = \kappa_{Au} \partial_\perp T(s^-, t) \\ T(s^+, t) = T(s^-, t) \end{cases} \tag{4}$$

where the Au and m subscripts refer to gold and medium and s^+ and s^- refer to the outer and inner parts of the interface position. The first boundary condition (third line in eq 4) ensures heat flux conservation at the GNR interface. No interface resistivity due to molecular coating is considered. Table 1 shows thermal constants for gold and some typical mediums.

The heat power density $p(r, t)$ in the first line in eq 4 is the heat power dissipated in the GNR (or the absorbed energy) per unit volume (V_{GNR} is the GNR volume). In the case of femtosecond-pulsed illumination, the heat power depends on the irradiance $I(t)$ and is calculated as

$$p(r, t) = \frac{\sigma_{abs} I(t)}{V_{GNR}} \tag{5}$$

where σ_{abs} is the optical absorption cross section of the GNR. A good estimation of this parameter is obtained from ref 24 considering a rodlike particle as a prolate spheroid.

As the electron−phonon thermalization occurs much faster than the external heat diffusion, the GNR absorbs the energy in a short time and reaches higher temperature values than in the CW laser case for the same average irradiance before dissipating the heat to the environment. This initial maximum temperature increment can be estimated as[1]

$$\Delta T_p = \frac{\sigma_{abs} E_p}{\rho_{Au} c_{Au} V_{GNR}} \tag{6}$$

where $E_p = \langle I \rangle / f_r$ is the pulse energy, $\langle I \rangle$ is the average irradiance, and f_r is the laser repetition rate. It is seen from eq 6 that the maximum temperature increment in the pulsed excitation case does not depend on the thermal properties of the environment but only on its permittivity through the absorption cross section.

As the set of eq 4 has no analytical solution, we solved it numerically by a finite difference scheme, with a regular spatiotemporal discretization in a cubic box of 300 nm side with the GNR centered at the origin. A constant room temperature was imposed on the boundary of the box. The absorption cross section was calculated at λ = 400 nm for a GNR with the average dimensions given in Figure 1. In Figure 3, we show the time evolution of the GNR temperature after a single femtosecond-pulse absorption considering different surrounding media. The small differences in the initial temperature are proportional to the differences in the medium permittivity, i.e., on the optical cross section. However, this instantaneous heating depends almost exclusively on the pulse energy. Besides that, the GNR cools down in a characteristic time that depends on the medium thermal conductivity and is related to the heat flux across the gold−medium interface. For example, thermal conductivity is 1 order of magnitude smaller for air than for water or glass, giving slower heat dissipation. This behavior is different from that in the CW irradiation case, where the heat dissipation time is inversely proportional to the

DOI: 10.1021/acs.jpcc.8b09458
J. Phys. Chem. C 2018, 122, 29598−29606

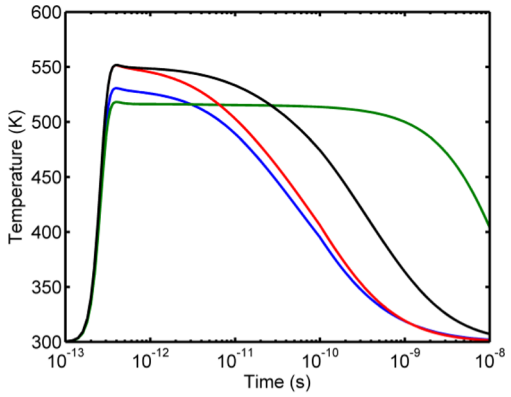

Figure 3. Temperature evolution of an average GNR during and after the absorption of a light pulse of 1.6 mW/μm^2 at 400 nm. The GNR is immersed in different media: water (blue), air (green), glass (red), and PMMA (black).

medium thermal diffusivity $\alpha = \kappa/\rho c$. Table 2 shows the calculated initial temperature increases ΔT_p (using eq 6 and solving numerically eq 4) and characteristic dissipation times τ_p for different environments, considering a GNR of average dimensions irradiated with an average irradiance of 1.6 mW/μm^2 (pulse energy of 2.4 pJ).

Table 2. Calculated Temperature Parameters of a GNR in a Single Femtosecond-Pulse Absorption[a]

	water	air	glass	PMMA
ΔT_p (eq 6)	233 °C	220 °C	254 °C	254 °C
ΔT_p	231 °C	218 °C	251 °C	252 °C
τ_p	0.12 ns	13.6 ns	0.13 ns	0.54 ns

[a]Initial maximum temperature increases of a GNR of 123.5 × 27.7 nm^2 (average population size), calculated with eq 6 and obtained with heat transfer simulations (with very good agreement), and characteristic dissipation times to different environments, in the femtosecond-pulsed case ($\langle I \rangle$ = 1.6 mW/μm^2, λ = 400 nm).

We solve the same set of eq 4 but considering now a more realistic situation where the GNR is deposited on a glass substrate and surrounded by air. We consider here that the gold surface is in contact with 18% of glass and 82% of air, as reported in ref 33, being a crude estimation without considering the nature of the nanorod−substrate interaction. In this case of double-contact dissipating media, the heat transfer is dominated by the most extended and poorly conductive air interface, but the presence of glass reduces the characteristic dissipation time, as shown in Figure 4. In this case, we obtain an initial temperature increase of 224 °C and a characteristic dissipation time close to 2.9 ns. In the same figure, temperature maps are shown at successive times of 0.005, 0.1, 1, and 4 ns after the pulse absorption.

If the dissipation time is comparable to the repetition pulse period and, consequently, if the GNR does not completely cools down to room temperature before the next pulse arrives, there will be an additional integrated temperature increment (over several pulse periods) that corresponds to the value reached in a steady-state CW regime. This temperature increase, not considered in Figures 3 and 4, depends on the average irradiance, the GNR size, and the thermal conductivity of the environment, being smaller, for our sample and experimental setup parameters, than the temperature increment after each absorbed pulse.

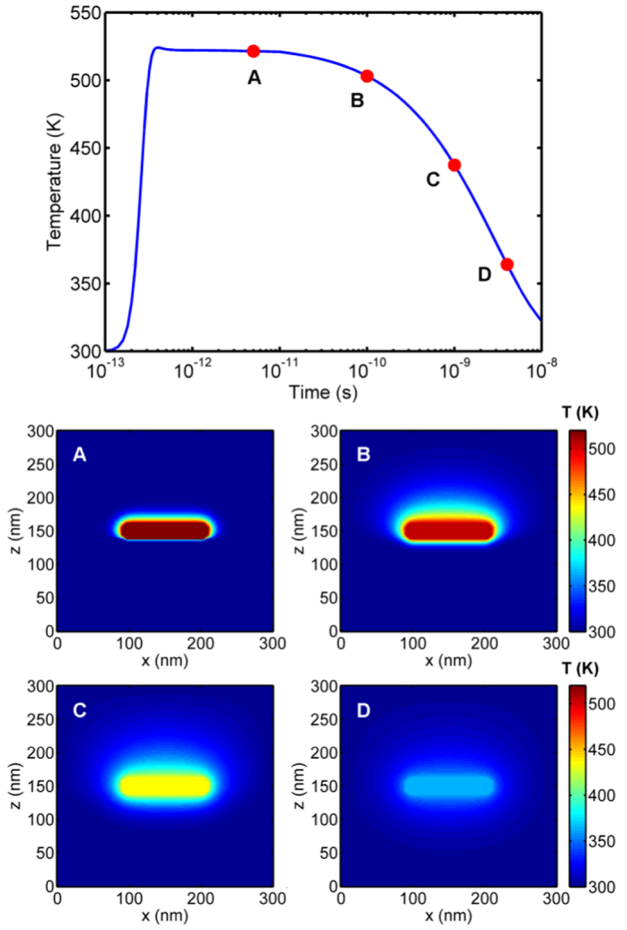

Figure 4. Temperature evolution of a GNR on glass, surrounded by air, during and after absorption of a light pulse of 1.6 mW/μm^2 at 400 nm, and temperature maps in a plane parallel to the main axis of the GNR and perpendicular to the glass surface, at times (A) 0.005, (B) 0.1, (C) 1, and (D) 4 ns after the pulse arrival, corresponding to the red dots in the curve.

If the GNR is now covered with a poly(methyl methacrylate) (PMMA) film, the dissipation time will be much smaller than in air because of its greater thermal conductivity. Thus, we expect in this case that this relatively rapid temperature decrease inhibits any appreciable surface atom diffusion and reshaping.

Photothermal Reshaping. The temperatures achieved in the GNRs with the pulse energies used in our experiments are well below the gold melting point, even for nanosized particles. Therefore, if there is any kind of reshaping in the nanorods that yields changes in the aspect ratio and in the mechanical vibrational frequencies, this must be based on mass diffusion at low temperatures. Monotonic increments in the extensional frequency as shown in Figure 2 imply a decrease in the aspect ratio, meaning that the mass diffusion must be happening from high- to low-curvature sites (from the tips to the waist), i.e., a curvature-driven atomic diffusion. Mullins and co-workers proposed a theory of capillarity-induced surface diffusion more than half a century ago to explain the observed blunting of the field-emission tips used in electron microscopes and the sintering of spheres.[27,28] The main concept of this theory is

DOI: 10.1021/acs.jpcc.8b09458
J. Phys. Chem. C 2018, 122, 29598−29606

that the atomic surface diffusion minimizes the surface energy of an object.

The surface flux $\mathbf{J}_s$ of atoms along an arbitrary surface under the assumption of isotropy of surface tension and surface self-diffusion can be written as

$$\mathbf{J}_s = -\frac{D_s \gamma \Omega \nu}{kT} \nabla_s K \tag{7}$$

where D_s is the surface self-diffusion coefficient, γ is the surface tension, Ω is the atomic volume, ν is the number of diffusing surface atoms per unit area, k is the Boltzmann constant, T is the temperature, and $\nabla_s K$ is the two-dimensional surface gradient of the surface curvature K. This surface flux should satisfy the continuity equation, $\partial n/\partial t + \nabla J_s = 0$, where $\partial n/\partial t$ represents the movement speed of a surface element in its outward normal direction. In the case of a body of revolution, we obtain the differential equation

$$\frac{\partial n}{\partial t} = \frac{B}{y}\frac{\partial}{\partial s}\left(y\frac{\partial K}{\partial s}\right) \tag{8}$$

where s is an arc element of the curve that generates the surface of revolution, y is the distance to the axis of revolution, and $B = D_s \gamma \Omega^{4/3}/kT$. Equation 8 describes the morphological changes of an arbitrary body of revolution by curvature-driven surface diffusion at any temperature. The surface self-diffusion coefficient D_s depends on temperature as

$$D_s(T) = D_0 \exp\left(-\frac{E_a}{kT}\right) \tag{9}$$

where D_0 is a constant (independent of sizes and temperature) and E_a is an activation energy. In the case of GNRs of length L, $D_0 = 4$ m^2/s and the activation energy E_a depends on its aspect ratio (AR) as $E_a = CL/(\mathrm{AR}^2 + 1)$, with $C = 2.6 \times 10^8$ eV/m, following the phenomenological values given by ref 32.

We solved eq 8 with a finite difference method, dividing the profile of a body of revolution into arc increments of equal size and assuming finite time intervals. Beginning with a prolate spheroid and after each time step, the normal distances traversed by each arc element define a new profile curve, which is obtained through parameterization equations.

If we use as input the profile curve of an average GNR with 123.5 nm length and 27.7 nm diameter, together with the temperature evolution during a pulse repetition period shown in Figure 4, corresponding to a rod on glass surrounded by air and irradiated by an average irradiance of 1.6 mW/μm^2, the calculations show very negligible photothermal reshaping after a single period but an appreciable surface diffusion after a very large number of periods. To see a greater change in a single pulse period, the activation energy must be lowered, for example reducing the rod size. In Figure 5, we show numerical results of the photothermal reshaping of a GNR with half a length and diameter of that of the average population size but the same aspect ratio, i.e., 4.5. The graphs show the AR curve variation superimposed to the temperature evolution of the GNR and the initial and final geometrical profiles.

To understand and reproduce the growing behavior of the extensional frequency measurements in our experiments, we have calculated the reshaping of a GNR on glass and surrounded by air with different average irradiance close to that used in our experiments. To obtain numerical results at long times as in Figure 2, it is necessary to increase the time step of each reshape calculation that resolves the temperature

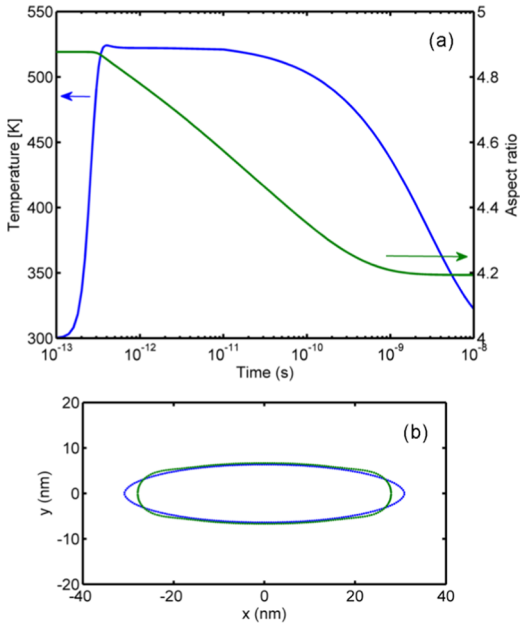

Figure 5. (a) Temperature evolution (blue curve) of an average synthesized GNR on glass and surrounded by air, irradiated by a femtosecond-pulsed laser of 1.6 mW/μm^2 at 400 nm, and AR variation (green, superimposed), due to reshaping, of a GNR with half the length and diameter but with the same temperature profile, to show the dramatic reshaping and change in AR in a single pulse period due to its lower activation energy. A GNR of average size has negligible reshaping during the same pulse duration (not showed here). (b) Initial and final geometrical profiles of the GNR with half the size.

evolution in each repetition period. To achieve this, we have checked numerically that the GNR reshaping (aspect ratio variation) during a sequence of many laser pulses with small temporal steps is completely equivalent to the GNR reshaping during a continuous wave irradiation with a laser power (or GNR steady-state temperature) that corresponds to an average surface self-diffusion coefficient D_s throughout the entire repetition period of the pulsed case. This equivalence was noticed in times on the order of milliseconds, and we extended it to longer times, in the seconds scale. In Figure 6, the reshaping (aspect ratio evolution) curves obtained at long times for a GNR irradiated with different average irradiance and the experimental aspect ratio points obtained from the extensional frequency measurements using eq 2 and assuming invariant volume can be seen, for a single GNR irradiated at an average irradiance of 1.4 mW/μm^2. There is a very good agreement between simulation and experimental results, suggesting that effectively the atomic surface diffusion is due to photothermal heating.

This correlation between extensional frequency measurements and calculated aspect ratios due to atomic surface diffusion is evident in most of the measured GNRs. However, in few cases, the frequency variations were greater than the expected ones, suggesting that there should be other possible causes adding temperature increments. Besides the GNR heating due to energy pulse absorption, additional overall heating of the sample would be possible because of a poor heat transfer at the macro scale, for example, due to a thermally isolated glass slide. Although SEM images showed that most of the irradiated GNRs were shortened by reshaping, some of them widened without losing length, with a consequent

DOI: 10.1021/acs.jpcc.8b09458
J. Phys. Chem. C 2018, 122, 29598−29606

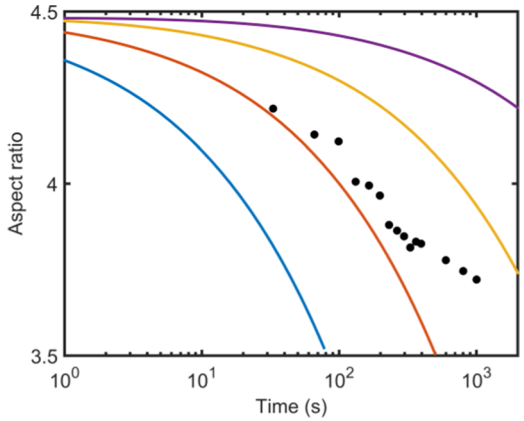

Figure 6. Aspect ratio calculations due to photothermal reshaping as a function of time of a GNR on glass surrounded by air and irradiated by a 400 nm pulsed laser with different irradiance: 1.6 (blue curve) mW/μm^2, 1.4 (orange) mW/μm^2, 1.2 (yellow) mW/μm^2, and 1.0 (violet) mW/μm^2, compared to those obtained from extensional frequency measurements in a single GNR.

flattening. This growth in the contact area with the substrate should increase the restitutive force and, consequently, increase the effective Young's modulus. Therefore, according to eq 2, this also produces an increment in the extensional mode frequency. To identify the cause of each kind of frequency variation, it would be necessary to obtain the scattering spectrum or the electron microscopy images of each individual GNR before and after irradiation. Also, the GNR size fluctuations (different initial aspect ratios correspond to different reshaping activation energies), the presence of an offset additional temperature after the first pulse, the contribution of the probe pulse extra heating, or the actual GNR position inside the beam spot should be considered. Important sources of fluctuations in experiments are the anchoring strength of the GNR to the surface, the contact area, and the molecular layer between the rod and the substrate. Each GNR may have a different thermal coupling to the substrate, which either affects or favors the heat diffusion to the environment. All of these factors mentioned, which were not considered in the theoretical treatment here, have less influence on the variations of the mechanical frequencies but should be taken into account to some extent, depending on the particular experimental case. The general conclusion of our results is that in any pump−probe experiment with metallic nanoantennas the nanoparticles suffer reshaping even for heating well below the melting temperature, allowing a sufficient time to elapse. These kinds of experiments are usually very lengthy because of the low signal-to-noise ratio, so the time scales that we present here are the typical ones.

As a final remark, we propose a way to reduce the photothermal reshaping of the GNRs based on the idea of favoring the heat transfer from the rod to the surroundings, by enclosing the nanoparticle into a medium of greater thermal conductivity than that of air. An easy way to do it is by depositing a polymer thin film over the sample by spin-coating. This approach is supported by results reported on surface-coated GNRs that increase the colloidal stability and can greatly reduce the reshaping behavior, under higher temperatures or higher irradiance than the ones used in this work.[34−38] These surface-coated GNRs (with silica and other heat-conducting materials) retain their optical properties at much higher fluences than bare GNRs, and their coatings could also restrict the mobility of the surface gold atoms.

We have repeated the previous experiments getting the extensional mode frequencies of single GNRs but now coated with a PMMA film. In Figure 7a, the time evolution of the

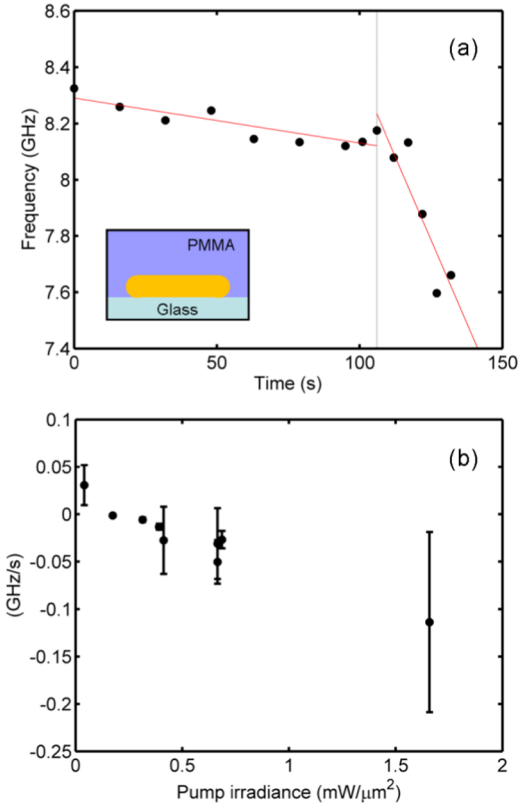

Figure 7. (a) Evolution of the extensional mode frequency of a single GNR deposited on glass and surrounded by a PMMA polymer film (see the inset) irradiated with a femtosecond-pulsed laser at 400 nm and an irradiance of 0.17 mW/μm^2 before the vertical dotted line and 0.69 mW/μm^2 after it. Notice the frequency decrease in time, with a higher rate at higher irradiance (red lines are only guides to the eye). This decrease cannot be attributed to a GNR photothermal reshaping because it would imply an aspect ratio growth. All measured GNRs showed a similar behavior, except in the very low irradiance case. (b) Average variation of the extensional frequency per unit time for 9 PMMA-coated GNRs. A monotonic variation of the frequency with the pump irradiance can be seen, which suggests an increasing elasticity of PMMA with temperature.

frequency for one of the single PMMA-coated GNRs is shown and for a long-time experiment. The first observation is that for GNRs within the same size population as in our previous study, the frequency of the extensional mode is greater than that in the case of air. This is because the assumptions made in the theory presented in eqs 1 and 2 are no longer valid. Indeed, the nanoparticle is now surrounded by a viscoelastic medium that will affect both the value of the frequencies of the mechanical modes of oscillation and its quality factors. In this article, we did not model this latter case and only pointed out that the frequencies start from a higher value than in the previous case.

Figure 7a shows that for the PMMA-coated case the frequency reduces as the time passes, as opposed to the case of nanorods surrounded by air (reduction of the frequency would imply an increase in the aspect ratio). This means that in this

DOI: 10.1021/acs.jpcc.8b09458
J. Phys. Chem. C 2018, 122, 29598−29606

case reshaping does not take place or that if it is competing with another effect, at least, the reshaping does not dominate. Also, from Figure 7a, it is evident that when the irradiance is increased (at about 100 s) the frequency shift per unit time increases as well. A more general result is shown in Figure 7b, where the frequency variations per unit time of 9 GNRs irradiated with different irradiance are shown. A linear dependence between the incident irradiance and the frequency shift per unit time is clearly observable. This result suggests a dependence of the GNR frequency on the mechanical properties of the polymer, which soften with the temperature increment, and as a consequence, the restitutive elastic force from the local environment is reduced. Again, if there is any photothermal reshaping of the nanoparticle, it seems negligible compared to this mechanical change of its close environment. Numerical surface diffusion calculations with PMMA-coated GNRs showed no appreciable reshaping because of the shorter dissipation time (with respect to air, see Figure 3), which is a consequence of the greater thermal conductivity of PMMA. Thus, this polymer coating technique on nanostructured samples is a simple and suitable method for slowing down photothermal reshaping.

CONCLUSIONS

We have presented in this work the generation and detection of mechanical modes of oscillation in plasmonic nanoparticles and used them to monitor the photothermal reshaping occurring in gold nanorods (GNRs), for long experimental times and various irradiation powers. Two-color pump−probe experiments and numerical simulations on single GNRs are in excellent agreement to show that in the case of nanorods surrounded by air there is an increment of the extensional mode frequency because of the photothermal reshaping produced by atomic surface diffusion. In the case of PMMA-coated GNRs, an opposite behavior was observed, showing a marked lowering of the frequency. In this case, there are no traces of reshaping, which make the polymer coating an easy resource for the metallic nanoantennas not to undergo changes in a usually long time-resolved type of experiment. As a final conclusion, we should say that even with low irradiation powers and for usual measuring times the effect of reshaping must be considered important and kept controlled in any experiment with plasmonic nanoantennas.

AUTHOR INFORMATION

Corresponding Author

*E-mail: ascarpettini@frd.utn.edu.ar.

ORCID

Alberto F. Scarpettini: 0000-0003-0630-2782

Notes

The authors declare no competing financial interest.

ACKNOWLEDGMENTS

This work was partially supported by PIP No. 112 201301 00619, UBACyT Proyecto No. 20020130100775BA, and PID-UTN 3541.

REFERENCES

(1) Baffou, G.; Rigneault, H. Femtosecond-Pulsed Optical Heating of Gold Nanoparticles. *Phys. Rev. B* **2011**, *84*, No. 035415.

(2) Richardson, H. H.; Carlson, M. T.; Tandler, P. J.; Hernandez, P.; Govorov, A. O. Experimental and Theoretical Studies of Light-to-Heat Conversion and Collective Heating Effects in Metal Nanoparticle Solutions. *Nano Lett.* **2009**, *9*, 1139−1146.

(3) Zijlstra, P.; Tchebotareva, A. L.; Chon, J. W. M.; Gu, M.; Orrit, M. Acoustic Oscillations and Elastic Moduli of Single Gold Nanorods. *Nano Lett.* **2008**, *8*, 3493−3497.

(4) Yu, K.; Zijlstra, P.; Sader, J. E.; Xu, Q.-H.; Orrit, M. Damping of Acoustic Vibrations of Immobilized Single Gold Nanorods in Different Environments. *Nano Lett.* **2013**, *13*, 2710−2716.

(5) Hartland, G. V. Coherent Excitation of Vibrational Modes in Metallic Nanoparticles. *Annu. Rev. Phys. Chem.* **2006**, *57*, 403−430.

(6) Jais, P. M.; Murray, D. B.; Merlin, R.; Bragas, A. V. Metal Nanoparticle Ensembles: Tunable Laser Pulses Distinguish Monomer from Dimer Vibrations. *Nano Lett.* **2011**, *11*, 3685−3689.

(7) Crut, A.; Maioli, P.; Del Fatti, N.; Vallée, F. Acoustic Vibrations of Metal Nano-Objects: Time-Domain Investigations. *Phys. Rep.* **2015**, *549*, 1−44.

(8) Pelton, M.; Wang, Y.; Gosztola, D.; Sader, J. E. Mechanical Damping of Longitudinal Acoustic Oscillations of Metal Nanoparticles in Solution. *J. Phys. Chem. C* **2011**, *115*, 23732−23740.

(9) Ruijgrok, P. V.; Zijlstra, P.; Tchebotareva, A. L.; Orrit, M. Damping of Acoustic Vibrations of Single Gold Nanoparticles Optically Trapped in Water. *Nano Lett.* **2012**, *12*, 1063−1069.

(10) Chang, W. S.; Wen, F.; Chakraborty, D.; Su, M. N.; Zhang, Y.; Shuang, B.; Nordlander, P.; Sader, J. E.; Halas, N. J.; Link, S. Tuning the Acoustic Frequency of a Gold Nanodisk through its Adhesion Layer. *Nat. Commun.* **2015**, *6*, No. 7022.

(11) Hu, M.; Wang, X.; Hartland, G. V.; Mulvaney, P.; Perez Juste, J.; Sader, J. E. Vibrational Response of Nanorods to Ultrafast Laser Induced Heating: Theoretical and Experimental Analysis. *J. Am. Chem. Soc.* **2003**, *125*, 14925−14933.

(12) Wang, L.; Takeda, S.; Liu, C.; Tamai, N. Coherent Acoustic Phonon Dynamics of Gold Nanorods and Nanospheres in a Poly(vinyl alcohol) Matrix and Their Temperature Dependence by Transient Absorption Spectroscopy. *J. Phys. Chem. C* **2014**, *118*, 1674−1681.

(13) Mohamed, M. B.; Ismail, K. Z.; Link, S.; El-Sayed, M. A. Thermal Reshaping of Gold Nanorods in Micelles. *J. Phys. Chem. B* **1998**, *102*, 9370−9374.

(14) Link, S.; Burda, C.; Nikoobakht, B.; El-Sayed, M. A. Laser-Induced Shape Changes of Colloidal Gold Nanorods Using Femtosecond and Nanosecond Laser Pulses. *J. Phys. Chem. B* **2000**, *104*, 6152−6163.

(15) Takahashi, H.; Niidome, T.; Nariai, A.; Niidome, Y.; Yamada, S. Photothermal Reshaping of Gold Nanorods Prevents further Cell Death. *Nanotechnology* **2006**, *17*, 4431−4435.

(16) Horiguchi, Y.; Honda, K.; Kato, Y.; Nakashima, N.; Niidome, Y. Photothermal Reshaping of Gold Nanorods Depends on the Passivating Layers of the Nanorod Surfaces. *Langmuir* **2008**, *24*, 12026−12031.

(17) Liu, Y.; Mills, E. N.; Composto, R. J. Tuning Optical Properties of Gold Nanorods in Polymer Films through Thermal Reshaping. *J. Mater. Chem.* **2009**, *19*, 2704−2709.

(18) Ng, K. C.; Cheng, W. Fine-Tuning Longitudinal Plasmon Resonances of Nanorods by Thermal Reshaping in Aqueous Media. *Nanotechnology* **2012**, *23*, No. 105602.

(19) Gordel, M.; Olesiak-Banska, J.; Matczyszyn, K.; Nogues, C.; Buckle, M.; Samoc, M. Post-Synthesis Reshaping of Gold Nanorods Using a Femtosecond Laser. *Phys. Chem. Chem. Phys.* **2014**, *16*, 71−78.

(20) González-Rubio, G.; Díaz-Núñez, P.; Rivera, A.; Prada, A.; Tardajos, G.; González-Izquierdo, J.; Bañares, L.; Llombart, P.; Macdowell, L. G.; Alcolea Palafox, M.; et al. Femtosecond Laser Reshaping yields Gold Nanorods with Ultranarrow Surface Plasmon Resonances. *Science* **2017**, *358*, 640−644.

(21) Harris-Birtill, D.; Singh, M.; Zhou, Y.; Shah, A.; Ruenraroengsak, P.; Gallina, M. E.; Hanna, G. B.; Cass, A. E. G.; Porter, A. E.; Bamber, J.; et al. Gold Nanorod Reshaping in Vitro and in Vivo Using a Continuous Wave Laser. *PLoS One* **2017**, *12*, No. e0185990.

DOI: 10.1021/acs.jpcc.8b09458
J. Phys. Chem. C 2018, 122, 29598−29606

(22) Ye, X.; Zheng, C.; Chen, J.; Gao, Y.; Murray, C. B. Using Binary Surfactant Mixtures to Simultaneously Improve the Dimensional Tunability and Monodispersity in the Seeded Growth of Gold Nanorods. *Nano Lett.* **2013**, *13*, 765−771.
(23) Gutiérrez, M. V.; Paredes, M. Y.; Scarpettini, A. F. Controlled Coverage of Glass Substrates with Metallic Nanorods. *Rev. Mater.* **2015**, *20*, 731−738.
(24) Bohren, C. F.; Huffman, D. R. *Absorption and Scattering of Light by Small Particles*; John Wiley: NY, 1983.
(25) Kreibig, U.; Vollmer, M. *Optical Properties of Metal Clusters*; Springer: Berlin, 1995.
(26) Shabana, A. A. *Vibration of Discrete and Continuous Systems*; Springer-Verlag: NY, 1997.
(27) Nichols, F. A.; Mullins, W. W. Morphological Changes of a Surface of Revolution Due to Capillarity-Induced Surface Diffusion. *J. Appl. Phys.* **1965**, *36*, 1826−1835.
(28) Mullins, W. W. Mass-Transport at Interfaces in Single-Component Systems. *Metall. Mater. Trans. A* **1995**, *26*, 1917−1929.
(29) Herring, C. Some Theorems on the Free Energies of Crystal Surfaces. *Phys. Rev.* **1951**, *82*, 87−93.
(30) Göbel, H.; von Blanckenhagen, P. A Study of Surface Diffusion on Gold with an Atomic Force Microscope. *Surf. Sci.* **1995**, *331−332*, 885−890.
(31) Huang, W.; Qian, W.; El-Sayed, M. A. Photothermal Reshaping of Prismatic Au Nanoparticles in Periodic Monolayer Arrays by Femtosecond Laser Pulses. *J. Appl. Phys.* **2005**, *98*, No. 114301.
(32) Taylor, A. B.; Siddiquee, A. M.; Chon, J. W. M. Below Melting Point Photothermal Reshaping of Single Gold Nanorods Driven by Surface Diffusion. *ACS Nano* **2014**, *8*, 12071−12079.
(33) Qin, F.; Cui, X.; Ruan, Q.; Lai, Y.; Wang, J.; Ma, H.; Lin, H.-Q. Role of Shape in Substrate-Induced Plasmonic Shift and Mode Uncovering on Gold Nanocrystals. *Nanoscale* **2016**, *8*, 17645−17657.
(34) Chen, Y.-S.; Frey, W.; Kim, S.; Homan, K.; Kruizinga, P.; Sokolov, K.; Emelianov, S. Enhanced Thermal Stability of Silica-Coated Gold Nanorods for Photoacoustic Imaging and Image-Guided Therapy. *Opt. Express* **2010**, *18*, 8867−8878.
(35) Canpean, V.; Gabudean, A. M.; Astilean, S. Enhanced Thermal Stability of Gelatin Coated Gold Nanorods in Water Solution. *Colloids Surf., A* **2013**, *433*, 9−13.
(36) Gergely-Fülöp, E.; Zámbó, D.; Deák, A. Thermal Stability of Mesoporous Silica-Coated Gold Nanorods with Different Aspect Ratios. *Mater. Chem. Phys.* **2014**, *148*, 909−913.
(37) Moon, H.; Kumar, D.; Kim, H.; Sim, C.; Chang, J.-H.; Kim, J.-M.; Kim, H.; Lim, D.-K. Amplified Photoacoustic Performance and Enhanced Photothermal Stability of Reduced Graphene Oxide Coated Gold Nanorods for Sensitive Photoacoustic Imaging. *ACS Nano* **2015**, *9*, 2711−2719.
(38) Albrecht, W.; Deng, T.-S.; Goris, B.; van Huis, M. A.; Bals, S.; van Blaaderen, A. Single Particle Deformation and Analysis of Silica-Coated Gold Nanorods before and after Femtosecond Laser Pulse Excitation. *Nano Lett.* **2016**, *16*, 1818−1825.

DOI: 10.1021/acs.jpcc.8b09458
J. Phys. Chem. C 2018, 122, 29598−29606